arXiv:1302.6925v2 [nucl-th] 3 Mar 2013

Equation of state of hypernuclear matter: impact of hyperon–scalar-meson couplings

Giuseppe Colucci and Armen Sedrakian
Institute for Theoretical Physics, J. W. Goethe-University, D-60438 Frankfurt-Main, Germany

We study the equation of state and composition of hypernuclear matter within a relativistic density functional theory with density-dependent couplings. The parameter space of hyperon–scalar-meson couplings is explored by allowing for mixing and breaking of SU(6) symmetry, while keeping the nucleonic coupling constants fixed. The subset of equations of state, which corresponds to small values of hyperon–scalar-meson couplings allows for massive $M \leq 2.25 M_\odot$ compact stars; the radii of hypernuclear stars are within the range 12-14 km. We also study the equation of state of hot neutrino-rich and neutrinoless hypernuclear matter and confirm that neutrinos stiffen the equation of state and dramatically change the composition of matter by keeping the fractions of charged leptons nearly independent of the density prior to the onset of neutrino transparency. We provide piecewise-polytropic fits to six representative equations of state of hypernuclear matter, which are suitable for applications in numerical astrophysics.

PACS numbers: 97.60.Jd,26.60.Kp,14.20.Jn,26.60.-c

I. INTRODUCTION

The integral parameters of compact stars depend on their equation of state (hereafter EoS) at high densities. Measurements of pulsar masses in binaries provide the most valuable information on the underlying EoS because these, being deduced from binary system parameters, are model independent within a given theory of gravity [1]. The recent discovery of a compact star with a mass of 1.97 $M_\odot$ (PSR J1614-2230) which sets an observationally "clean" lower bound on the maximum mass of a compact star via the measured Shapiro delay [2], spurred an intensive discussion of the phase structure of dense matter in compact stars consistent with this limit [3–27]. Pulsar radii have been extracted, e.g., from modeling the X-ray binaries under certain reasonable model assumptions, but the uncertainties are large [28–31]. An example, that we will use in our analysis, is the pulse phase-resolved X-ray spectroscopy of PSR J0437-4715, which sets a lower limit on the radius of a 1.76 $M_\odot$ solar mass compact star $R > 11$ km within 3σ error [31].

Large masses and radii are an evidence for the relative stiffness of the EoS of dense matter at high densities. Large densities may require substantial population of heavy baryons (hyperons), because these become energetically favorable once the Fermi energy of neutrons becomes of the order of their rest mass. Their onset then reduces the degeneracy pressure of a cold thermodynamic ensamble and softens effectively the EoS of dense matter. This decreases the maximum mass of a compact stars to values which contradict the observation of massive compact stars in Nature. This controversy between the theory and observations is the essence of the "hyperonization puzzle" in compact stars.

Although the emergence of heavy baryons (mainly $\Sigma^\pm$ and Λ hyperons) was considered even before the discovery of pulsars and their identification with neutron stars [32], their existence in the cores of neutron stars is still elusive. Seminal work on interacting hyperonic matter was carried early after the discovery of pulsars [33, 34]. Systematic studies of interacting dense hypernuclear matter were carried out with the advent of relativistic density functional methods [35–44], for reviews see [45, 46]. Most of the these works predicted masses that are not much larger than the canonical mass of a neutron star (in contradiction with modern observations). Masses on the order of $\leq 1.8 M_\odot$ were obtained later on in non-relativistic phenomenological models [47]. Fully microscopic models based on hyperon-nucleon potentials, which include the repulsive three-body forces, predict low maximal masses for hypernuclear stars [48, 49].

Finite temperature hyperonic matter in the presence of thermal bath of neutrinos may differ significantly from cold hypernuclear matter found in evolved neutron stars. Previous studies [50–53] showed that the EoS becomes stiffer, the deleptonizing effect of charged hyperons at zero temperature is removed in the presence of neutrinos and the sequence in which charged hyperons appear changes.

In this work we contribute to the investigation of "hyperonization puzzle" by studying the parameter space of the couplings of hyperons to the light scalar octet of mesons. The parameter space is partially motivated by the hypernuclear potentials as well as investigations of the external field QCD sum rules that involve SU(6) symmetry breaking and mixing [54, 55]. Because the structure and even content of the scalar mesons is still a subject of discussion it appears necessary to investigate this particular domain of hypernuclear physics with respect to the consistency with the compact star observations. Conversely, as we show below, the considered parameter space can in fact account for massive hyperonic compact stars, thus providing a possible solution to the "hyperonization puzzle".

To study the EoS of hypernuclear matter we use a model based on relativistic density functional theory of Walecka and a density dependent parameterization of the nucleon–meson couplings of Ref. [56]. The EoS and composition of matter will be studied both in the zero temperature limit relevant to mature compact stars, as well as at finite temperatures relevant for their hot proto-neutron star stage of evolution. In the latter case we assume neutrino-rich matter in β-equilibrium and explore the effects of finite temperature and neutrino content on the stiffness and composition of matter. We confirm the general features found in the previous analysis [50–53] and provide a detailed account of the EoS and composition of matter within our model.

This paper is structured as follows. In Sec. II we discuss the theoretical set-up of the relativistic density functional theory. The parameterization of the coupling constants of the theory is discussed in Sec. III. Sec. IV is devoted to the discussion of the choice of the hyperon-meson coupling constants. We present our results in Sec. V. Finally, our conclusions are collected in Sec. VI.

II. THEORETICAL MODEL

The relevant degrees of freedom in nuclear matter at high density are nucleons and hyperons. In particular, we choose as degrees of freedom of our relativistic mean field model the baryon octet ($J^P = \frac{1}{2}^+$), and we study the interaction of these fields with the isoscalar-scalar, σ, isoscalar-vector, ω_μ, and isovector-vector, $\boldsymbol{\rho}_\mu$, mesons. Besides these fields, we also consider the presence of leptons, e^-, μ^-. In the case of finite temperature matter, which describes proto-neutron star matter, the model has the neutrino degrees of freedom, because they are expected to be trapped in a proto-neutron star within the first minute after its birth. The introduction of additional variables, the neutrino chemical potentials, requires additional constraints, which we provide by fixing the lepton fractions, Y_{Ll}, appropriate for conditions prevailing during the evolution of a proto-neutron star [51].

The relativistic Lagrangian reads

$$\begin{aligned}\mathcal{L} &= \sum_B \bar\psi_B\Big[\gamma^\mu\left(i\partial_\mu - g_{\omega BB}\omega_\mu - \frac{1}{2}g_{\rho BB}\boldsymbol{\tau}\cdot\boldsymbol{\rho}_\mu\right)\\ &- (m_B - g_{\sigma BB}\sigma)\Big]\psi_B + \frac{1}{2}\partial^\mu\sigma\partial_\mu\sigma - \frac{1}{2}m_\sigma^2\sigma^2\\ &- \frac{1}{4}\omega^{\mu\nu}\omega_{\mu\nu} + \frac{1}{2}m_\omega^2\omega^\mu\omega_\mu - \frac{1}{4}\boldsymbol{\rho}^{\mu\nu}\boldsymbol{\rho}_{\mu\nu} + \frac{1}{2}m_\rho^2\boldsymbol{\rho}^\mu\cdot\boldsymbol{\rho}_\mu\\ &+ \sum_\lambda \bar\psi_\lambda(i\gamma^\mu\partial_\mu - m_\lambda)\psi_\lambda - \frac{1}{4}F^{\mu\nu}F_{\mu\nu}, \qquad (1)\end{aligned}$$

where the B-sum is over the $J^P = \frac{1}{2}^+$ baryon octet, ψ_B are the baryonic Dirac fields with masses m_B. The interaction is mediated by the σ, ω_μ and $\boldsymbol{\rho}_\mu$ meson fields with the $\omega_{\mu\nu}$ and $\boldsymbol{\rho}_{\mu\nu}$ field strength tensors and masses m_σ, m_ω, and m_ρ. The baryon-meson coupling constants are denoted by g_{BBm} (their numerical value will be discussed in Sec. III below). The λ-sum in Eq. (1) runs over the leptons e^-, μ^-, ν_e and ν_μ with masses m_λ and the last term is the electromagnetic energy density. The contribution of neutrinos to the sum above is included only at non-zero temperature, when they are trapped in stellar matter and form a statistical ensamble in equilibrium. In mature compact stars at zero temperature the neutrinos do not contribute to the thermodynamical quantities of matter because they are out of equilibrium and their chemical potential vanishes.

The Lagrangian density (1) yields the pressure and the energy density, which at finite temperature read respectively

$$\begin{aligned}P &= -\frac{m_\sigma^2}{2}\sigma^2 + \frac{m_\omega^2}{2}\omega_0^2 + \frac{m_\rho^2}{2}\rho_{03}^2 + \frac{1}{3}\sum_B \frac{2J_B+1}{2\pi^2}\\ &\times \int_0^\infty \frac{k^4\ dk}{(k^2+m_B^{*2})^{1/2}}\left[f(E_k-\mu_B^*) + f(E_k+\mu_B^*)\right]\\ &+ \frac{1}{3\pi^2}\sum_\lambda \int_0^\infty \frac{k^4\ dk}{(k^2+m_\lambda^2)^{1/2}}\left[f(E_k-\mu_\lambda) + f(E_k+\mu_\lambda)\right]\end{aligned} \qquad (2)$$

and

$$\begin{aligned}\epsilon &= \frac{m_\sigma^2}{2}\sigma^2 + \frac{m_\omega^2}{2}\omega_0^2 + \frac{m_\rho^2}{2}\rho_{03}^2 + \sum_B \frac{2J_B+1}{2\pi^2}\\ &\times \int_0^\infty dk\ k^2(k^2+m_B^{*2})^{1/2}\left[f(E_k-\mu_B^*) + f(E_k+\mu_B^*)\right]\\ &+ \sum_\lambda \int_0^\infty \frac{dk}{\pi^2}k^2(k^2+m_\lambda^2)^{1/2}\left[f(E_k-\mu_\lambda) + f(E_k+\mu_\lambda)\right],\end{aligned} \qquad (3)$$

where σ, ω_0 and ρ_{03} are the nonvanishing mesonic mean fields, J_B is the baryon degeneracy factor, $m_B^* = m_B - g_{\sigma BB}$ is the effective baryon mass, $\mu_B^* = \mu_B - g_{\omega BB}\omega_0 - g_{\rho BB}I_3\rho_3^0$ is the baryon chemical potential including the time component of the fermion self-energy, I_3 is the third component of baryon isospin and $f(y) = [1+\exp(y/T)]^{-1}$ is the Fermi distribution function with T being the temperature.

At non-zero temperature the net entropy of the matter is the sum of the baryon contribution

$$\begin{aligned}S_B &= -\sum_B \frac{2J_B+1}{2\pi^2}\int_0^\infty dk k^2\Big\{\Big[f(E_k-\mu_B^*)\ln f(E_k-\mu_B^*)\\ &+ \bar f(E_k-\mu_B^*)\ln \bar f(E_k-\mu_B^*)\Big] + (\mu_B^*\to -\mu_B^*)\Big\}\end{aligned} \qquad (4)$$

and the lepton contribution

$$\begin{aligned}S_L &= -\sum_\lambda \int_0^\infty \frac{dk}{\pi^2}\Big[f(E_k-\mu_\lambda)\ln f(E_k-\mu_\lambda)\\ &+ \bar f(E_k-\mu_\lambda)\ln \bar f(E_k-\mu_\lambda)\Big],\end{aligned} \qquad (5)$$

where $\bar f(y) = 1 - f(y)$. The free-energy density is then given by

$$F = \epsilon - T(S_B + S_L). \qquad (6)$$

III. DENSITY-DEPENDENT PARAMETRIZATION DD-ME2

Below, we shall work with a density dependent parameterization, which is designed to account in an economical manner the many-body correlations that arise beyond the mean-field approximation. The density dependence of the coupling constant accounts for the influence of the medium on the scattering of baryons. We choose to work with the DD-ME2 parameterization, designed in Ref. [56], which introduces an explicit density dependence in the nucleon-meson couplings $g_{NN\sigma}$, $g_{NN\omega}$ and $g_{NN\rho}$. The phenomenological Ansatz for the density dependence for the σ and ω_μ meson coupling constants is

$$g_{NNi}(\rho_B) = g_{NNi}(\rho_0) h_i(x), \qquad i = \sigma,\ \omega, \tag{7}$$

where ρ_B is the baryon density,

$$h_i(x) = a_i \frac{1 + b_i(x + d_i)^2}{1 + c_i(x + d_i)^2} \tag{8}$$

is a function of $x = \rho_B/\rho_0$, ρ_0 is the nuclear saturation density. The parameters in (8) are not independent. The five constraints $h_i(1) = 1, h''_\sigma(1) = h''_\omega(1), h''_i(0) = 0$, reduce the number of independent parameters to three. Three additional parameters in the isoscalar-scalar channel are $g_{NN\sigma}(\rho_0)$, $g_{NN\omega}(\rho_0)$ and m_σ, the mass of the phenomenological σ meson. Microscopic calculations show that the $\boldsymbol{\rho}_\mu$-meson coupling vanishes at high densities [57]. Therefore, instead of the Ansatz (8) one can use a simpler exponential form of density dependence

$$g_{NN\rho}(\rho_B) = g_{NN\rho}(\rho_0) \exp[-a_\rho(x - 1)]. \tag{9}$$

Thus, the parameterization we will be using has in total eight parameters, which are adjusted to reproduce the properties of symmetric and asymmetric nuclear matter, binding energies, charge radii, and neutron radii of spherical nuclei. The parameters of the DD-ME2 effective interaction are shown in Table I.

TABLE I: Meson masses and their couplings to the baryons in DD-ME2 parametrization.

	σ	ω	ρ
m_i [MeV]	550.1238	783.0000	763.0000
$g_{NNi}(\rho_0)$	10.5396	13.0189	3.6836
a_i	1.3881	1.3892	0.5647
b_i	1.0943	0.9240	—
c_i	1.7057	1.4620	—
d_i	0.4421	0.4775	—

When the coupling constants are density dependent, the thermodynamical consistency (specifically the energy conservation and fulfillment of the Hugenholtz-van Hove theorem) require the inclusion of the so-called rearrangement self-energy [58]. This contributes to the pressure, but not to the energy of the system. The pressure becomes

$$P_r \ = \ P + \rho_B \Sigma_r, \tag{10}$$

where the rearrangement self-energy, Σ_r, is given by

$$\Sigma_r = \frac{\partial g_{NN\omega}}{\partial \rho_B} \omega_0 \rho_B - \frac{\partial g_{NN\sigma}}{\partial \rho_B} \sigma \rho_S, \tag{11}$$

where ρ_S is the scalar density. It can be verified that the contribution from the rearrangement self-energy restores the thermodynamical relation

$$P_r = \rho_B^2 \frac{\partial}{\partial \rho_B} \left(\frac{\epsilon}{\rho_B} \right), \tag{12}$$

which is otherwise violated. Below we shall always consider the pressure including the rearrangement term and will drop the subscript r.

IV. HYPERON-MESON COUPLING CONSTANTS

To extend the description of matter to full baryon octet we need the hyperon-meson coupling constants. Because the information on the properties of hypernuclear matter is far less extensive than for nucleons their values can not be fixed with certainty and several approaches have been used in the literature.

One way to fix these couplings is to consider the SU(3)-flavor symmetric model, namely the octet model. In this model the degrees of freedom are represented by the lowest non-trivial irreducible representation (IR) of the symmetry group which is physically possible, $\{8\}$, that is the baryon octet and the mesonic octet.

Let us consider first the interaction between the baryon octet, $J^P = \frac{1}{2}^+$, and the vector meson octet, $J^P = 1^-$. Within the assumption of SU(3)-flavor symmetry, one can express the meson-baryon coupling constants in terms of only two parameters [59], the nucleon–$\boldsymbol{\rho}_\mu$ meson coupling constant $g_{NN\rho}$ and the $F/(F + D)$ ratio of the vector octet α_V:

$$\begin{aligned}
&g_{NN\rho} = g_8, && g_{\Xi\Xi\rho} = -g_8(1 - 2\alpha_V),\\
&g_{\Sigma\Sigma\rho} \ = 2g_8\alpha_V, && g_{\Lambda\Lambda\rho} = 0,\\
&g_{NN\omega_8} = \frac{1}{\sqrt{3}} g_8(4\alpha_V - 1), && g_{\Xi\Xi\omega_8} = -\frac{1}{\sqrt{3}} g_8(1 + 2\alpha_V),\\
&g_{\Sigma\Sigma\omega_8} \ = \frac{2}{\sqrt{3}} g_8(1 - \alpha_V), && g_{\Lambda\Lambda\omega_8} = -\frac{2}{\sqrt{3}} g_8, (1 - \alpha_V),
\end{aligned} \tag{13}$$

where we have shown only the coupling constants relevant for our model. The vector-meson dominance model [60] predicts $\alpha_V = 1$, which is a result of the universal coupling of the $\boldsymbol{\rho}_\mu$ meson to the isospin current. This result is also in agreement with recent QCD sum rules calculations [55]. Therefore, we set $\alpha_V = 1$ in hyperon–$\boldsymbol{\rho}_\mu$ meson coupling constants in Eq. (13), i.e.,

$$g_{\Xi\Xi\rho} = g_8, \qquad g_{\Sigma\Sigma\rho} = 2g_8, \qquad g_{\Lambda\Lambda\rho} = 0. \tag{14}$$

To describe the mixing between the singlet and the octet members of the vector nonet, one has to introduce two additional parameters - the flavor singlet coupling constant, g_1, and the vector mixing angle, θ_V. Therefore, the coupling of the baryon to the physical ω_μ-meson state now reads

$$g_{BB\omega} = \cos\theta_V g_1 + \sin\theta_V g_{BB\omega_8}. \tag{15}$$

It is widely accepted that the mixing between non-strange and strange quark wave functions in the ω and ϕ mesons is ideal [61, 62]. In this limit $\tan\theta_V = 1/\sqrt{2}$ and assuming again $\alpha_V = 1$ we obtain the baryon–ω_μ meson couplings as

$$\begin{aligned} \frac{g_{NN\omega}}{\sin\theta_V} &= \sqrt{2}g_1 + \sqrt{3}g_8, \\ \frac{g_{\Xi\Xi\omega}}{\sin\theta_V} &= \sqrt{2}g_1 - \sqrt{3}g_8, \\ \frac{g_{\Sigma\Sigma\omega}}{\sin\theta_V} &= \frac{g_{\Lambda\Lambda\omega}}{\sin\theta_V} = \sqrt{2}g_1. \end{aligned} \tag{16}$$

Next we assume that the nucleons do not couple to pure strange mesons (ϕ_μ). One then obtains the relation between the singlet and the octet coupling constants [63]:

$$g_1 = \sqrt{6}\, g_8, \tag{17}$$

which allows one to eliminate g_1 from Eqs. (16). Thus, the hyperon–ω_μ meson coupling constants can be related to the nucleon one

$$g_{\Xi\Xi\omega} = \frac{1}{3} g_{NN\omega}, \quad g_{\Sigma\Sigma\omega} = g_{\Lambda\Lambda\omega} = \frac{2}{3} g_{NN\omega}. \tag{18}$$

We are now left with the hyperon-scalar meson (σ) coupling constants. In order to fix these parameters, we consider the relations among the coupling constants for the scalar octet [54], which are given [in analogy with the relations for the vector meson octet in Eq. (13)] by

$$\begin{aligned} &g_{NNa_0} = g_S, && g_{\Xi\Xi a_0} = -g_S(1-2\alpha_S), \\ &g_{\Sigma\Sigma a_0} = 2g_S\alpha_S, && g_{\Lambda\Lambda a_0} = 0, \\ &g_{NN\sigma_8} = \frac{1}{\sqrt{3}}g_S(4\alpha_S - 1), && g_{\Xi\Xi\sigma_8} = -\frac{1}{\sqrt{3}}g_S(1+2\alpha_S), \\ &g_{\Sigma\Sigma\sigma_8} = \frac{2}{\sqrt{3}}g_S(1-\alpha_S), && g_{\Lambda\Lambda\sigma_8} = -\frac{2}{\sqrt{3}}g_S(1-\alpha_S). \end{aligned} \tag{19}$$

The mixing between the singlet and the octet states of the scalar nonet is given by

$$g_{BB\sigma} = \cos\theta_S g_1 + \sin\theta_S g_{BB\sigma_8}. \tag{20}$$

Then, the σ meson-baryon coupling constants are

$$\begin{aligned} g_{NN\sigma} &= \cos\theta_S\ g_1 + \sin\theta_S\ (4\alpha_S - 1)g_S/\sqrt{3}, && (21) \\ g_{\Lambda\Lambda\sigma} &= \cos\theta_S\ g_1 - 2\sin\theta_S\ (1-\alpha_S)g_S/\sqrt{3}, && (22) \\ g_{\Sigma\Sigma\sigma} &= \cos\theta_S\ g_1 + 2\sin\theta_S\ (1-\alpha_S)g_S/\sqrt{3}, && (23) \\ g_{\Xi\Xi\sigma} &= \cos\theta_S\ g_1 - \sin\theta_S\ (1+2\alpha_S)g_S/\sqrt{3}. && (24) \end{aligned}$$

Combining the couplings, we obtain

$$\begin{aligned} g_{\Lambda\Lambda\sigma} + g_{\Sigma\Sigma\sigma} &= 2\cos\theta_S\ g_1, && (25) \\ g_{NN\sigma} + g_{\Xi\Xi\sigma} &= 2\cos\theta_S\ g_1 - 2\sin\theta_S\ (1-\alpha_S)g_S/\sqrt{3} \\ &= \cos\theta_S\ g_1 + g_{\Lambda\Lambda\sigma}. && (26) \end{aligned}$$

Eliminating g_1 from these expressions we obtain a relation

$$2(g_{NN\sigma} + g_{\Xi\Xi\sigma}) = 3g_{\Lambda\Lambda\sigma} + g_{\Sigma\Sigma\sigma}, \tag{27}$$

which is valid for arbitrary values of the four parameters α_S, g_1, g_S and θ_S. In particular, it is satisfied for the values of the coupling constants in the SU(6) symmetric quark model. Indeed, the latter model assumes that the σ meson is a pure up and down state, therefore for strangeness -1 Λ and Σ baryons $g_{\Lambda\Lambda\sigma} = g_{\Sigma\Sigma\sigma} = \frac{2}{3}g_{NN\sigma}$, whereas for strangeness -2 Ξ baryons $g_{\Xi\Xi\sigma} = \frac{1}{3}g_{NN\sigma}$. Due to the constraint (27) the parameter space of our model is spanned by three out of the four parameters α_S, g_1, g_S and θ_S. Further constraints on the parameter space can be placed on account that the hyperon coupling constants must be positive and less than the nucleon coupling constant. This implies two additional constraints, which can be translated into constraints on the range of variability of the hyperon–scalar meson coupling constants. Indeed, by expressing one of the hyperon coupling constants, say $g_{\Xi\Xi\sigma}$, in terms of the others with the help of Eq. (27) one finds

$$g_{\Xi\Xi\sigma} = \frac{1}{2}(3g_{\Lambda\Lambda\sigma} + g_{\Sigma\Sigma\sigma}) - g_{NN\sigma}, \tag{28}$$

and therefore, by requiring that

$$0 \le g_{\Xi\Xi\sigma} \le g_{NN\sigma}, \tag{29}$$

one is left with the following two simultaneous inequalities

$$g_{NN\sigma} \le \frac{1}{2}(3g_{\Lambda\Lambda\sigma} + g_{\Sigma\Sigma\sigma}) \le 2g_{NN\sigma}. \tag{30}$$

To explore the parameter space spanned by the hyperon-σ meson couplings we use the following approach. We fix the value of $g_{\Lambda\Lambda\sigma}$ at the value provided by the Nijmegen Soft Core (NSC) hypernuclear potential model of Ref. [64] and vary the range of couplings $g_{\Sigma\Sigma\sigma}$ within the limits provided by Eq. (30). The corresponding $g_{\Xi\Xi\sigma}$ couplings are found from Eq. (28). Analogously, to explore the range of admissible $g_{\Lambda\Lambda\sigma}$ couplings, we next fix the value of $g_{\Sigma\Sigma\sigma}$ to the value provided by the NSC model and change the $g_{\Lambda\Lambda\sigma}$ coupling within a range which keeps the values of $g_{\Xi\Xi\sigma}$ consistent with Eq. (29). The parameter space is further limited by the requirement that the maximal values of $g_{\Lambda\Lambda\sigma}$ and $g_{\Sigma\Sigma\sigma}$ should be below their values in the SU(6) symmetric model. This latter constraint is motivated physically by our search for a stiff EoS of hypernuclear matter.

V. RESULTS

The matter in evolved compact stars is charge neutral and in β-equilibrium. These two conditions are imposed when computing the EoS at zero temperature. For young neutron stars at non-zero temperature a thermal ensamble of neutrinos should be included for temperatures $T \geq 5$ MeV. In this case a common practice is to vary the lepton fraction of matter in a certain range compatible with astrophysical simulations. We shall treat below these distinct cases in turn.

A. Zero temperature

We start the discussion of our results by comparing the EoS of purely nucleonic matter, computed using density-dependent (DD) ME2 parameterization of nuclear matter, to the EoS where interacting hyperons are added with couplings taken according to SU(6) quark model, see Fig. 1. The appearance of hyperons, which is triggered by the fact that the cost of having a hyperon heavier than a nucleon is energetically more favorable than a neutron at the top of the Fermi sea, always softens the EoS. Because in our search the coupling constants are bound from above by their values in the SU(6) model, these two EoS correspond to the stiffest and softest EoS in our collection.

Our next step is to explore the impact of the variation of the hyperon–scalar meson coupling on the EoS. As explained in the previous Sec. IV, we will keep the hyperon–vector meson couplings fixed at the values given by Eqs. (14) and (18) and vary the hyperon–scalar meson coupling constants in the range and manner defined above.

The left panel of Fig. 2 shows the dependence of the EoS of hypernuclear matter on variations of the coupling constant in the range $0.26 \leq x_{\Sigma\Sigma\sigma} \leq 0.66$ at fixed $x_{\Lambda\Lambda\sigma} = 0.58$ (a value that corresponds to the NSC model), where $x_{HH\sigma} = g_{HH\sigma}/g_{NN\sigma}$ is the ratio of the hyperon-σ and the nucleon-σ coupling constants. The resulting EoS cover the shaded area, which is bound by the two EoS corresponding to the limiting values of the parameter $g_{\Sigma\Sigma\sigma}$; in addition we show the special case where the $g_{\Sigma\Sigma\sigma}$ parameter is fitted to reproduce the empirical value of the Σ-hyperon potential in nuclear matter at saturation $U_\Sigma = 30$ MeV according to

$$U_\Sigma = \frac{g_{\Sigma\Sigma\sigma}}{g_{NN\sigma}}\langle\sigma\rangle + \frac{g_{\Sigma\Sigma\omega}}{g_{NN\omega}}\langle\omega\rangle, \tag{31}$$

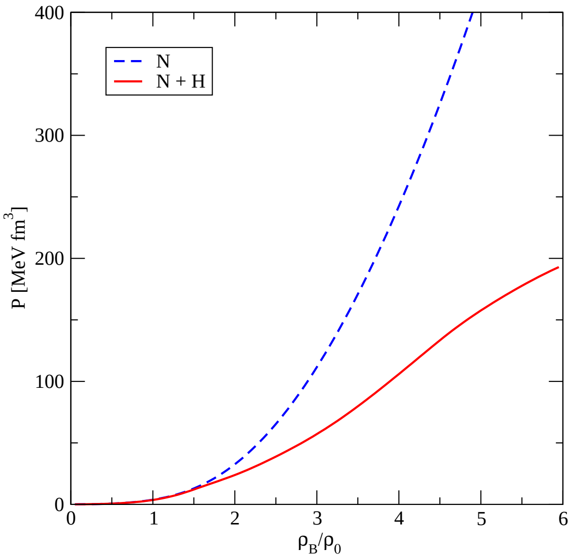

FIG. 1: (Color online) Equations of state of nuclear (dashed, blue online) and hypernuclear (solid, red online) matter. The coupling constants for nuclear matter correspond to density-dependent (DD) ME2 parametrization of Ref. [56]. The coupling constants of hyperons are related to the nucleonic ones according to the SU(6) symmetric quark model. The density is normalized to the nuclear saturation density $\rho_0 = 0.152$ fm^{-3} in the DD ME2 parametrization.

where $\langle \dots \rangle$ refers to a mean-field value of the field. The right panel of Fig. 2 shows the dependence of the EoS of hypernuclear matter on variations of the $g_{\Lambda\Lambda\sigma}$ coupling constant in the range $0.52 \leq x_{\Lambda\Lambda\sigma} \leq 0.66$ at fixed $x_{\Sigma\Sigma\sigma} = 0.448$ (as implied by the NSC model). The set of resulting EoS covers the shaded area; we also show explicitly the limiting cases as well as the special case, where the $g_{\Lambda\Lambda\sigma}$ coupling is fitted to reproduce the Λ-hyperon potential in nuclear matter at saturation $U_\Lambda = -28$ MeV according to an equation analogous to Eq. (31). As expected, the reduction of the hyperon couplings stiffens the EoS. The stiffest hypernuclear EoS in this set corresponds to the values of couplings $x_{\Sigma\Sigma\sigma} = 0.448$ and $x_{\Lambda\Lambda\sigma} = 0.52$.

Fig. 3 shows the particle fractions of fermions, defined as the ratio of particle number densities to the baryon number density for the limiting cases of the SU(6) quark model couplings and the stiffest hypernuclear EoS. There are a number of features that are common to the both EoS. The appearance of Σ^- hyperons, which compensate the positive change of the nuclear matter and excess of negative isospin of the neutrons, is favored at low density. They contribute to the suppression and eventual extinction of electron and muon populations at large densities, i.e., the matter becomes deleptonized. Once the increasing with density population of Σ^- hyperons reaches the population of protons, the charge neutrality prevents further increase of Σ^- hyperons. Instead, an excess of neutral Λ hyperons builds up and dominates the hyperon population at asymptotically large densities. In the case of softer EoS (left panel of Fig. 3) the deleptonization

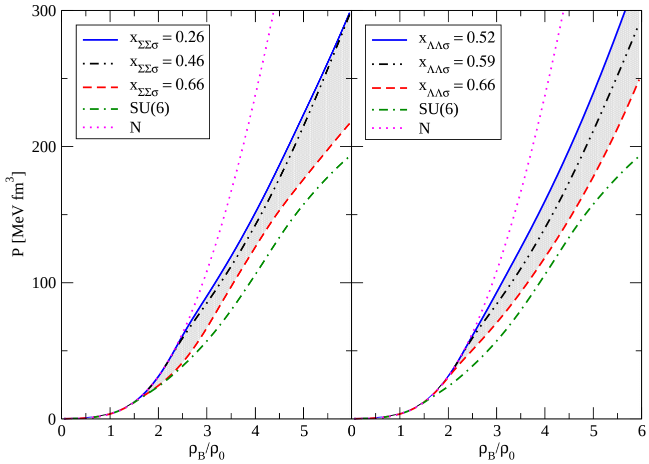

FIG. 2: (Color online) Equations of state of hypernuclear matter for a range of values of hyperon-σ meson couplings defined in terms of $x_{HH\sigma} = g_{HH\sigma}/g_{NN\sigma}$, $H \in \Lambda, \Sigma$. The nucleonic EoS (dotted line, magenta online) and hyperonic EoS with SU(6) quark model couplings (dot-dashed line, green online) are shown as a reference. The nucleonic coupling constants correspond to the DD-ME2 parametrization [56]; the hyperon-vector meson couplings are fixed as explained in the text. Left panel: we assume $x_{\Lambda\Lambda\sigma} = 0.58$, as in the NSC potential model, and a range $0.26 \leq x_{\Sigma\Sigma\sigma} \leq 0.66$ which generates the shaded area. Right panel: we assume $x_{\Sigma\Sigma\sigma} = 0.448$, as in the NSC potential model, and a range $0.26 \leq x_{\Lambda\Lambda\sigma} \leq 0.66$. The cases $x_{\Sigma\Sigma\sigma} = 0.46$ (left panel) and $x_{\Lambda\Lambda\sigma} = 0.59$ (right panel), shown by dash-double-dotted (black online) lines, fit the depth of the potentials of the Σ^- and Λ hyperons in nuclear matter at saturation.

and onset of hyperons like $\Sigma^{0,+}$ and cascades $\Xi^{0,-}$ occurs at densities lower than in the case of the stiff EoS (right panel of Fig. 3). This is the consequence of the fact that the large hyperon-meson couplings favor the formation of hyperons, which in turn soften the EoS. Thus, the SU(6) quark model, with its large meson-hyperon couplings favors the onset of hyperons at low densities, which produces a soft EoS. Conversely, the stiffest EoS, which corresponds to small values of the hyperon-meson couplings, disfavors the onset of hyperons.

B. Finite temperatures

Compact stars become transparent to neutrinos after about a minute of formation in a supernova explosion. Prior to the neutrino-transparency era the star is hot, with temperatures of order of several tens of MeV and neutrinos are in equilibrium with matter. The neutrino thermal distribution is characterized by the neutrino chemical potential μ_ν and neutrino fraction $Y_\nu = n_\nu/n_B$, i.e., the ratio of the neutrino number density to the baryon number density. The neutrino fraction is commonly parameterized by specifying the lepton fraction for each flavor $Y_L = Y_l + Y_\nu$, where Y_l is the fraction of the charged leptons of given flavor. The relevant to proto-neutron stars range of lepton fraction is $0.1 \leq Y_L \leq 0.4$.

Figure 4 shows the EoS of hot hypernuclear matter in the cases when there is a thermal population of neutrinos with $0.1 \leq Y_L \leq 0.4$ (shaded area) and in the absence of neutrinos, i.e., $Y_\nu = 0$ and Y_l determined from β-equilibrium with $\mu_{\nu,l} = 0$, as in cold hypernuclear

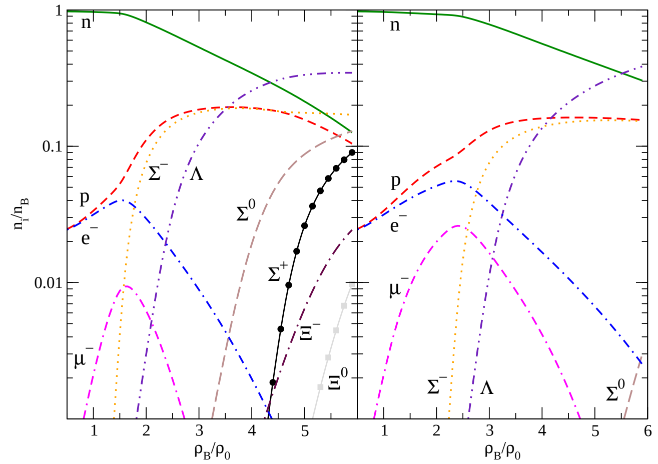

FIG. 3: (Color online) Particle fractions in hypernuclear matter at $T = 0$. Left panel: hyperon–scalar meson couplings are fixed as in the SU(6) symmetric quark model. Right panel: a stiff hypernuclear EoS from our parameter space with $x_{\Sigma\Sigma\sigma} = 0.448$ and $x_{\Lambda\Lambda\sigma} = 0.52$.

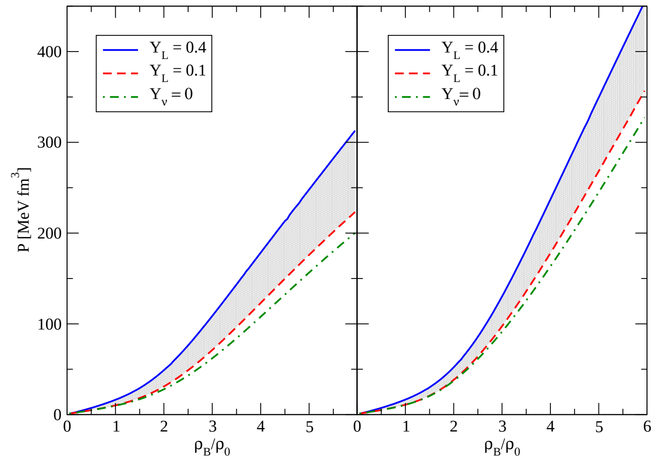

FIG. 4: (Color online) Equation of state of hypernuclear matter at $T = 50$ MeV with and without neutrinos. In the left panel the hyperon–scalar meson coupling constants are fixed by the SU(6) quark model, whereas in the right panel $g_{\Sigma\Sigma\sigma} = 0.448 g_{NN\sigma}$ and $g_{\Lambda\Lambda\sigma} = 0.52 g_{NN\sigma}$, which corresponds to the stiffest cold hypernuclear EoS considered. In each panel the dash-dotted line (green online) corresponds to the case without neutrinos. The shaded region shows the range of variation of each EoS when the lepton fraction is changed between the limiting cases $Y_L = 0.1$ (dashed, red online) and $Y_L = 0.4$ (solid, blue online).

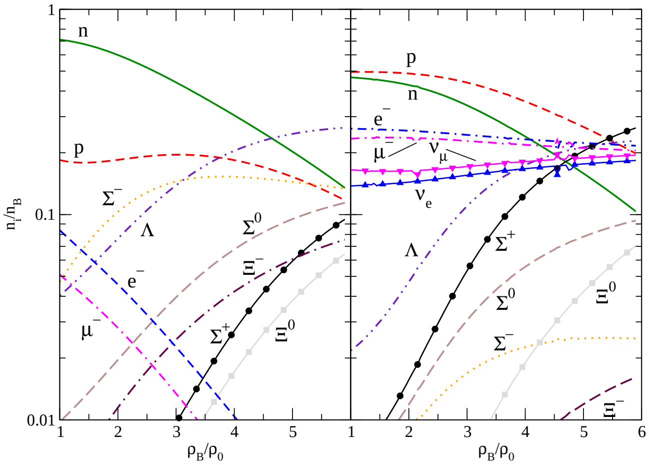

FIG. 5: (Color online) Particle fractions in hypernuclear matter at $T = 50$ MeV for a soft hypernuclear EoS with couplings fixed by SU(6) symmetric quark model; $Y_\nu = 0$ in the left panel and $Y_L = 0.4$ in the right panel.

matter. The influence of the neutrino population was considered for two parametrizations: one corresponds to the parameters implied by the SU(6) quark model and a soft EoS and another corresponds to $x_{\Sigma\Sigma\sigma} = 0.448$ and $x_{\Lambda\Lambda\sigma} = 0.52$ and a stiff EoS (see Fig. 2 for the $T = 0$ counterparts). It can be seen that the EoS is stiff when neutrinos are present ($Y_\nu \neq 0$) and the larger is the fraction of neutrinos, i.e. Y_L, the stiffer is the EoS. The stiffening of the EoS can be attributed to the fact that the thermal population of neutrinos adds its contribution to the pressure of matter. However, neutrinos stiffen the EoS also indirectly by changing the composition of matter. As seen in Figs. 5 and 6 the presence of neutrinos has a strong effect on charged leptons: the deleptonization effect observed in neutrino-less matter is reversed when neutrinos are present. As a consequence the Σ^- hyperons are disfavored in neutrino-rich matter. In fact the sequence of appearance of charged Σ hyperons is reversed (cf. the left and right panels of Fig. 5). Because neutrinos suppress the hyperon (predominantly Λ) fractions, the EoS is closer to the nucleonic one, which as we have seen, is always stiffer than the hypernuclear EoS. By comparing Figs. 5 and 6 one can access how various choices of the hyperon–scalar-meson couplings influence the composition of matter. The general trend, observed at $T = 0$ (Fig. 3), persists at non-zero temperatures, i.e., the thresholds for the onset of the various hyperons shift to higher densities for smaller values of the couplings of hyperons to the scalar mesons. The models with high values of these couplings are softer and more hyperon-rich as the ones with smaller values of these couplings.

C. Polytropic fits to the EoS

Numerical relativity and astrophysics problems frequently require a simple parametrization of the EoS of matter at zero temperature. The polytropic form of the EoS has been one of the common choices and, more recently, *piecewise-polytropic* EoS were used to construct accurate representations of microscopic EoS [65]. We shall use below the following representation

$$P = \sum_{i=1}^{4} K_i \rho^{\Gamma_i} \theta(\rho - a_i\rho_0)\theta(b_i\rho_0 - \rho), \qquad (32)$$

where Γ_i is the polytropic index, K_i is a dimensionful constant, ρ_0 is the saturation density. These parameters are used to fit the EoS within a density interval, whose lower and upper boundaries are specified by the parameters a_i and b_i. The six different EoS that were parametrized using Eq. (32) include a nuclear EoS, a hypernuclear EoS based on the SU(6) symmetric quark model, and four additional EoS with $x_{\Sigma\Sigma\sigma}$ and $x_{\Lambda\Lambda\sigma}$ from the range discussed above. Table II lists the fitting parameters. The polytropic representation above should be matched to an EoS of matter in the crust of a neutron star at the density $0.5\rho_0$ (assumed to be the largest density in the crust). To optimize the fit, the density segments were chosen to optimally reflect the changes in the EoS; for example one knot, in the case of hypernuclear EoS, is chosen to be the density of the onset of hyperons. The change of the polytropic index with density is consistent with the expectation that as matter becomes more relativistic, the polytropic index decreases.

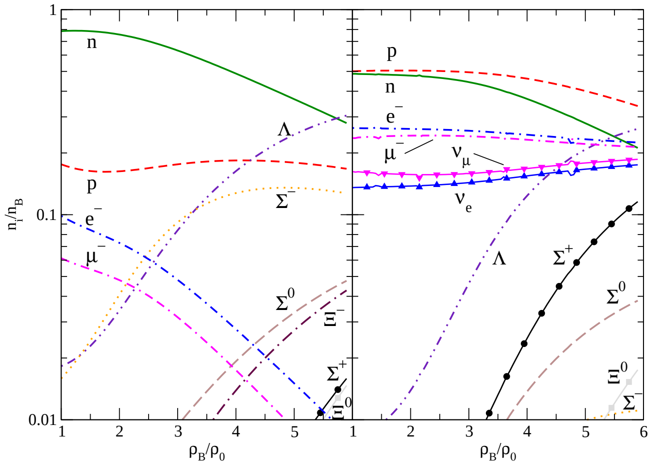

FIG. 6: (Color online) Same as in Fig. 5, but for a stiff hypernuclear EoS with couplings $x_{\Sigma\Sigma\sigma} = 0.448$ and $x_{\Lambda\Lambda\sigma} = 0.52$.

TABLE II: Piecewise-polytropic parametrizations of various EoS according to Eq. (32). Set A corresponds to a pure nucleonic EoS. The hyperonic EoS with different values $x_{\Sigma\Sigma\sigma}$ and $x_{\Lambda\Lambda\sigma}$ are arranged as follows: set B: $x_{\Lambda\Lambda\sigma} = 0.52$ and $x_{\Sigma\Sigma\sigma} = 0.448$, set C: $x_{\Lambda\Lambda\sigma} = 0.66$ and $x_{\Sigma\Sigma\sigma} = 0.448$, set D: $x_{\Lambda\Lambda\sigma} = 0.58$ and $x_{\Sigma\Sigma\sigma} = 0.26$, set E: $x_{\Lambda\Lambda\sigma} = 0.58$ and $x_{\Sigma\Sigma\sigma} = 0.66$. Set F refers to the hyperonic EOS with $x_{HH\sigma}$ fixed to the values of the SU(6) symmetric quark model. The dimensionful constant K_i is given in units of MeV fm$^{3+3\Gamma_i}$.

i	K_i	Γ_i	a_i	b_i	K_i	Γ_i	a_i	b_i
	set A				set B			
1	3.68535	2.86324	0.5	1.35	3.56837	3.12001	0.5	2.5
2	3.73399	3.07344	1.35	3	7.66522	2.27431	2.5	3
3	6.89825	2.54758	3	5	12.0670	1.86718	3	4
4	13.2029	2.16247	5	10	12.9132	1.81431	4	6
	set C				set D			
1	3.76801	2.98366	0.5	2.25	3.55834	3.12437	0.5	2.5
2	9.15775	1.86209	2.25	3	9.18876	2.08451	2.5	3
3	9.64638	1.80967	3	5	12.9246	1.77419	3	5
4	7.79875	1.94152	5	6	15.7905	1.64781	5	6
	set E				set F			
1	4.24406	2.50544	0.5	3.5	4.01772	2.62586	0.5	2
2	9.27949	1.88033	3.5	4.25	5.49227	2.13420	2	4.25
3	18.9055	1.38903	4.25	5	10.5763	1.68309	4.25	5
4	25.6369	1.19845	5	6	24.7673	1.15400	5	6

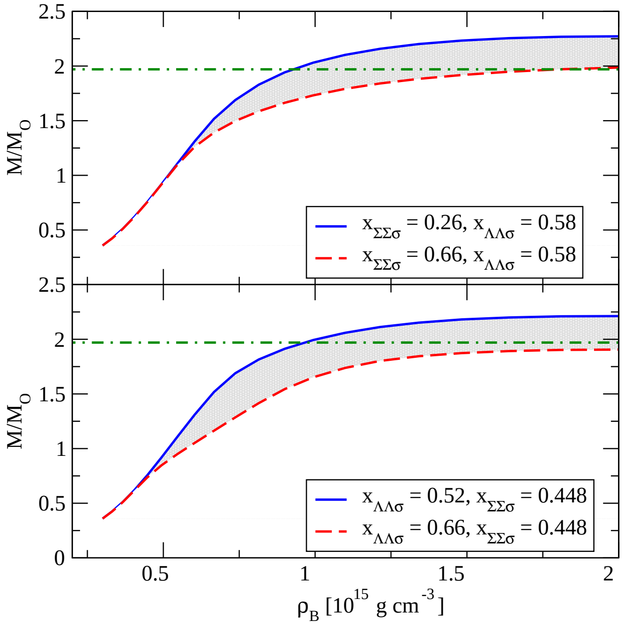

FIG. 7: (Color online) Dependence of the gravitational mass of compact hypernuclear stars on central density at zero temperature. The solid (blue online) and dashed (red online) lines show the limiting cases of parameter space as indicated in the panels. The dash-dotted (green online) line shows the observational lower limit on the maximum mass $1.97M_\odot$.

D. Stellar structure

The spherically symmetric solutions of Einstein's equations for self-gravitating fluids are given by the well-known Tolman-Oppenheimer-Volkoff equations, which can be integrated for any given EoS. It is convenient to parametrize the equilibrium sequences of non-rotating configurations at zero temperature by their central density. A universal feature of these solutions is the existence of a maximum mass for any EoS, i.e., as the central density is increased a sequence reaches the configuration with the maximum mass and the stars with larger central densities are unstable towards gravitational collapse. A condition of stability for a sequence of configurations is $dM/d\rho_c \geq 0$, i.e., the mass should be an increasing function of the central density. Alternatively, the stability analysis of the lowest-order harmonics of pulsation modes (e.g. the fundamental radial pulsations) allows to access the stability of a configuration, for these are damped for stable stars and increase exponentially for unstable stars.

The range of considered hypernuclear EoS translates into the band of stable configurations shown in Fig. 7. The configuration containing hypernuclear matter branch off from the purely nuclear ones as the central density is increased beyond the threshold density for appearance of hyperons in matter. The gravitational masses of hypernuclear stars increase with the density indicating a stable branch of these objects. The maximum masses are $\leq 2.25M_\odot$ and are reached for central densities of order $7\rho_0$. Most of the sequences generated by the parameter space of the couplings considered are compatible with the observational bound $M/M_\odot \geq 1.97$. There is also room left for larger mass stars to allow for statistical distribution of the masses of neutron stars beyond this limit. Note that $1.4M_\odot$ canonical mass stars would be pure nucleonic for the stiffer subclass of EoS considered, whereas they would contain hypernuclear matter for the softer subclass; however for all the EoS considered, the stars with $M > 1.5M_\odot$ contain hypernuclear matter.

In Fig. 8 we show the mass-radius relationship for the hypernuclear sequences. The configurations with masses close to the maximum mass $M \simeq 2M_\odot$ have radii of $R \simeq 12$ km, whereas the canonical mass stars have radii of order 14 km. The figure also shows the bound, which predicts that PSR J0437-4715, being a $M = 1.76M_\odot$ neutron star, has a radius $R > 12.5$ km at 2σ level. Clearly, the hypernuclear stars are consistent with this observation. Finally we note that it is not excluded that the low-mass neutron stars with $M \sim 1.2M_\odot$ may already contain hypernuclear matter.

VI. CONCLUSIONS

Despite of decades long theoretical research on the hypernuclear matter, the appearance of hyperons in compact stars remains an open issue. While the recent as-

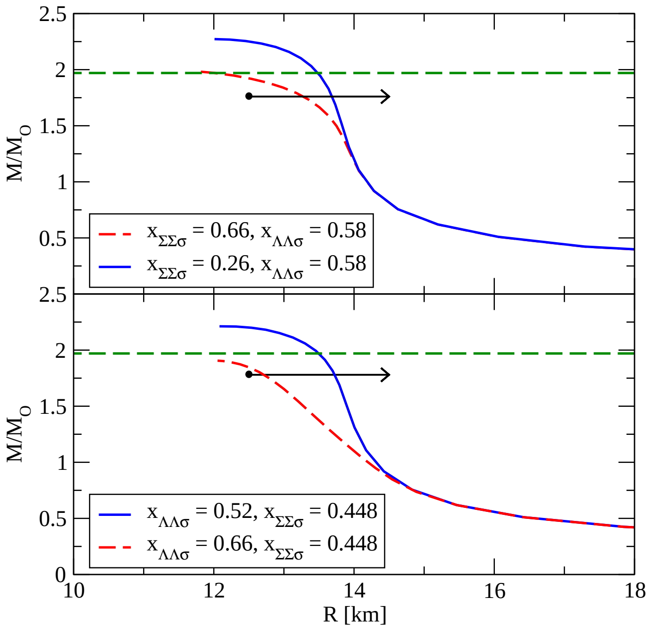

FIG. 8: (Color online) The mass–radius relations for compact hypernuclear stars at zero temperature. The labeling and parameter space is as in Fig. 7. The arrow shows the mass-radius constraint of Ref. [31] at 2σ level, which is $M = 1.76 M_\odot$ and $R \geq 12.5$ km.

trophysical measurements exclude a significant fraction of soft EoS, the hyperonization of dense nuclear matter remains a serious possibility. Our present study confirms this within a relativistic density functional approach to nuclear matter, where we investigated the impact of variation of the hyperon-scalar meson couplings on the EoS of hypernuclear matter. The range of found EoS is sufficiently stiff to produce heavy enough compact stars ($M \leq 2.25 M_\odot$). The radii of our sequences are located in the range of $12 \leq R \leq 14$ km. Piecewise-polytropic fits for six representative EoS are provided, which span the complete range of EoS from our parameter study.

The parameter space of couplings of hyperons to scalar mesons was explored holding density dependent nucleonic couplings fixed to their values suggested by the DD-ME2 parametrization of the nuclear density functional [56]. To allow for hyperonization in massive stars a requirement is to have small ratios of the hypernuclear to nuclear couplings, in particular, hyperons should be coupled to scalar mesons weaker than predicted by the SU(6) quark model.

Our study of the EoS and composition of matter at non-zero temperature and including thermal ensamble of neutrinos (present in a compact star during the first minute after birth) confirms that the neutrinos stiffen the high-density EoS and impact the charge lepton content of hypernuclear matter. Instead of deleptonization with increasing density, seen in neutrino-less matter, the abundances of charged leptons remain constant, which has the consequence that the thresholds for appearance of charged Σ's is reversed.

The hyperonic abundances found in our EoS are broadly consistent with the predictions of other (both early and recent) models. Indeed, these are determined by the hyperon mass spectrum and conditions of charge neutrality and β-equilibrium. By varying the scalar meson couplings, we showed that the stiffer the EoS the larger are the densities at which any type of hyperon appears. For example, substantial amounts of cascades appear already at densities of the order $(3-4)\rho_0$ for a soft EoS and only trace amounts for a stiff EoS. Furthermore, at non-zero temperatures the thresholds for the onset of hyperons are located at densities lower than those at zero temperature. It is evident that during the early cooling stage of a neutron star (the time period when the temperature drops from tens of MeV to a MeV and matter becomes transparent to neutrinos) a rearrangement of particle content of matter must take place.

Acknowledgments

We gratefully acknowledge the support by the HGS-HIRe graduate program at Frankfurt University (G. C.) and a collaborative research grant of the Volkswagen Foundation (A. S.). We thank B. Friman, D. H. Rischke, P. Ring, and D. Vretrenar for discussions and R. G. E. Timmermans for useful communications.

[1] M. Kramer, ArXiv e-prints (2012), arXiv:1211.2457 [astro-ph.HE] .
[2] P. B. Demorest, T. Pennucci, S. M. Ransom, M. S. E. Roberts, and J. W. T. Hessels, Nature (London) , **467**, 1081 (2010), arXiv:1010.5788 [astro-ph.HE] .
[3] M. C. Miller, Nature (London) , **467**, 1057 (2010).
[4] J. R. Stone, P. A. M. Guichon, and A. W. Thomas, ArXiv e-prints (2010), arXiv:1012.2919 [nucl-th] .
[5] I. Vidaña, D. Logoteta, C. Providência, A. Polls, and I. Bombaci, EPL (Europhysics Letters), **94**, 11002 (2011), arXiv:1006.5660 [nucl-th] .
[6] C.-Y. Ryu, C. H. Hyun, and C.-H. Lee, Phys. Rev. C , **84**, 035809 (2011), arXiv:1108.5843 [nucl-th] .
[7] L. Bonanno and A. Sedrakian, Astronomy&Astrophysics, **539**, A16 (2012), arXiv:1108.0559 [astro-ph.SR] .
[8] M. Bejger, J. L. Zdunik, P. Haensel, and M. Fortin, Astron.& Astrophys., **536**, A92 (2011), arXiv:1109.1179 [astro-ph.HE] .
[9] S. Weissenborn, D. Chatterjee, and J. Schaffner-Bielich, Nuclear Physics A, **881**, 62 (2012), arXiv:1111.6049 [astro-ph.HE] .
[10] R. Lastowiecki, D. Blaschke, H. Grigorian, and S. Typel,

ArXiv e-prints (2011), arXiv:1112.6430 [nucl-th] .
[11] S. Weissenborn, D. Chatterjee, and J. Schaffner-Bielich, Phys. Rev. C , **85**, 065802 (2012), arXiv:1112.0234 [astro-ph.HE] .
[12] M. Oertel, A. F. Fantina, and J. Novak, Phys. Rev. C , **85**, 055806 (2012), arXiv:1202.2679 [nucl-th] .
[13] R. Mallick, ArXiv e-prints (2012), arXiv:1207.4872 [astro-ph.HE] .
[14] K. Masuda, T. Hatsuda, and T. Takatsuka, Astrophys. J. , **764**, 12 (2013), arXiv:1205.3621 [nucl-th] .
[15] C. H. Lenzi and G. Lugones, Astrophys. J. , **759**, 57 (2012), arXiv:1206.4108 [astro-ph.SR] .
[16] V. Dexheimer, J. Steinheimer, R. Negreiros, and S. Schramm, Phys. Rev. C , **87**, 015804 (2013), arXiv:1206.3086 [astro-ph.HE] .
[17] F. Gulminelli, A. R. Raduta, and M. Oertel, Phys. Rev. C , **86**, 025805 (2012), arXiv:1206.4924 [nucl-th] .
[18] W.-Z. Jiang, B.-A. Li, and L.-W. Chen, Astrophys. J. , **756**, 56 (2012), arXiv:1207.1686 [astro-ph.SR] .
[19] F. Gulminelli, A. R. Raduta, J. Margueron, P. Papakonstantinou, and M. Oertel, ArXiv e-prints (2012), arXiv:1209.0270 [nucl-th] .
[20] J. L. Zdunik and P. Haensel, ArXiv e-prints (2012), arXiv:1211.1231 [astro-ph.SR] .
[21] P.-C. Chu and L.-W. Chen, ArXiv e-prints (2012), arXiv:1212.1388 [astro-ph.SR] .
[22] W.-Z. Jiang, R.-Y. Yang, and D.-R. Zhang, ArXiv e-prints (2012), arXiv:1212.3686 [nucl-th] .
[23] C. Providência and A. Rabhi, ArXiv e-prints (2012), arXiv:1212.5911 [nucl-th] .
[24] K. Masuda, T. Hatsuda, and T. Takatsuka, ArXiv e-prints (2012), arXiv:1212.6803 [nucl-th] .
[25] F. Gulminelli, A. R. Raduta, M. Oertel, and J. Margueron, ArXiv e-prints (2013), arXiv:1301.0390 [nucl-th] .
[26] A. Sedrakian, ArXiv e-prints (2013), arXiv:1301.2675 [astro-ph.HE] .
[27] F. Gulminelli, A.-R. Raduta, J. Margueron, P. Papakonstantinou, and M. Oertel, ArXiv e-prints (2013), arXiv:1302.3776 [nucl-th] .
[28] S. Guillot, R. E. Rutledge, and E. F. Brown, Astrophys. J. , **732**, 88 (2011), arXiv:1007.2415 [astro-ph.GA] .
[29] T. Güver, P. Wroblewski, L. Camarota, and F. Özel, Astrophys. J. , **719**, 1807 (2010), arXiv:1002.3825 [astro-ph.HE] .
[30] D. K. Galloway and N. Lampe, Astrophys. J. , **747**, 75 (2012), arXiv:1201.1680 [astro-ph.HE] .
[31] S. Bogdanov, Astrophys. J. , **762**, 96 (2013), arXiv:1211.6113 [astro-ph.HE] .
[32] V. A. Ambartsumyan and G. S. Saakyan, Astronomicheski Zhurnal, **37**, 193 (1960).
[33] H. A. Bethe and M. B. Johnson, Nuclear Physics A, **230**, 1 (1974).
[34] S. A. Moszkowski, Phys. Rev. D , **9**, 1613 (1974).
[35] N. K. Glendenning, Physics Letters B, **114**, 392 (1982).
[36] N. K. Glendenning, Astrophys. J. , **293**, 470 (1985).
[37] N. K. Glendenning, Zeitschrift fur Physik A Hadrons and Nuclei, **326**, 57 (1987).
[38] N. K. Glendenning, Zeitschrift fur Physik A Hadrons and Nuclei, **327**, 295 (1987).
[39] F. Weber and M. K. Weigel, Nuclear Physics A, **493**, 549 (1989).
[40] J. I. Kapusta and K. A. Olive, Physical Review Letters, **64**, 13 (1990).
[41] J. Ellis, J. I. Kapusta, and K. A. Olive, Nuclear Physics B, **348**, 345 (1991).
[42] N. K. Glendenning and S. A. Moszkowski, Physical Review Letters, **67**, 2414 (1991).
[43] P. J. Ellis, R. Knorren, and M. Prakash, Physics Letters B, **349**, 11 (1995), arXiv:nucl-th/9502033 .
[44] J. Schaffner and I. N. Mishustin, Phys. Rev. C , **53**, 1416 (1996), arXiv:nucl-th/9506011 .
[45] F. Weber, *Pulsars as astrophysical laboratories for nuclear and particle physics, Bristol, U.K.: Institute of Physics,* (1999).
[46] A. Sedrakian, Progress in Particle and Nuclear Physics, **58**, 168 (2007), arXiv:nucl-th/0601086 .
[47] S. Balberg, I. Lichtenstadt, and G. B. Cook, Astrophys. J. Suppl., **121**, 515 (1999), arXiv:astro-ph/9810361 .
[48] H.-J. Schulze and T. Rijken, Phys. Rev. C , **84**, 035801 (2011).
[49] D. Logoteta, I. Vidaña, C. Providência, A. Polls, and I. Bombaci, Journal of Physics Conference Series, **342**, 012006 (2012).
[50] I. L. Vartanian and N. K. Ovakimova, Soviet Astron., **21**, 727 (1977).
[51] J. A. Pons, S. Reddy, M. Prakash, J. M. Lattimer, and J. A. Miralles, Astrophys. J. , **513**, 780 (1999), arXiv:astro-ph/9807040 .
[52] I. Bednarek, M. Kęska, and R. Mańka, International Journal of Modern Physics D, **13**, 215 (2004).
[53] G. F. Burgio, H.-J. Schulze, and A. Li, Phys. Rev. C , **83**, 025804 (2011), arXiv:1101.0726 [astro-ph.SR] .
[54] G. Erkol, R. G. E. Timmermans, M. Oka, and T. A. Rijken, Phys. Rev. C , **73**, 044009 (2006), arXiv:nucl-th/0603058 .
[55] G. Erkol, R. G. E. Timmermans, and T. A. Rijken, Phys. Rev. C , **74**, 045201 (2006).
[56] G. A. Lalazissis, T. Nikšić, D. Vretenar, and P. Ring, Phys. Rev. C , **71**, 024312 (2005).
[57] S. Typel and H. H. Wolter, Nuclear Physics A, **656**, 331 (1999).
[58] C. Fuchs, H. Lenske, and H. H. Wolter, Phys. Rev. C , **52**, 3043 (1995), arXiv:nucl-th/9507044 .
[59] J. J. de Swart, Reviews of Modern Physics, **35**, 916 (1963).
[60] J. J. Sakurai, Annals of Physics, **11**, 1 (1960).
[61] KLOE Collaboration, F. Ambrosino, A. Antonelli, S. Bertolucci, C. Bini, C. Bloise, S. Bocchetta, F. Bossi, P. Branchini, G. Capon, T. Capussela, F. Ceradini, P. Ciambrone, E. De Lucia, A. De Santis, P. De Simone, G. De Zorzi, A. Denig, A. Di Domenico, C. Di Donato, B. Di Micco, M. Dreucci, G. Felici, and G. Xu, Journal of High Energy Physics, **7**, 105 (2009), arXiv:0906.3819 [hep-ph] .
[62] A. Kucukarslan and U.-G. Meißner, Modern Physics Letters A, **21**, 1423 (2006), arXiv:hep-ph/0603061 .
[63] C. B. Dover and A. Gal, Progress in Particle and Nuclear Physics, **12**, 171 (1984).
[64] P. M. M. Maessen, T. A. Rijken, and J. J. de Swart, Phys. Rev. C , **40**, 2226 (1989).
[65] J. S. Read, B. D. Lackey, B. J. Owen, and J. L. Friedman, Phys. Rev. D , **79**, 124032 (2009), arXiv:0812.2163 .